THE ANATOMICAL RECORD 293:1477–1491 (2010)

The Global Impact of Sutures Assessed in a Finite Element Model of a Macaque Cranium

QIAN WANG,[1*] AMANDA L. SMITH,[2] DAVID S. STRAIT,[2] BARTH W. WRIGHT,[3] BRIAN G. RICHMOND,[4,5] IAN R. GROSSE,[6] CRAIG D. BYRON,[7] AND URIEL ZAPATA[1,8]

[1]Division of Basic Medical Sciences, Mercer University School of Medicine, Macon, Georgia
[2]Department of Anthropology, University at Albany, Albany, New York
[3]Department of Anatomy, Kansas City University of Medicine and Biosciences, Kansas City, Missouri
[4]Department of Anthropology, Center for the Advanced Study of Hominid Paleobiology, The George Washington University, Washington DC
[5]Human Origins Program, National Museum of Natural History, Smithsonian Institution, Washington DC
[6]Department of Mechanical & Industrial Engineering, University of Massachusetts, Amherst, Massachusetts
[7]Department of Biology, Mercer University, Macon, Georgia
[8]Department of Mechanical Engineering, EAFIT University, Medellín, Colombia

ABSTRACT

The biomechanical significance of cranial sutures in primates is an open question because their global impact is unclear, and their material properties are difficult to measure. In this study, eight suture-bone functional units representing eight facial sutures were created in a finite element model of a monkey cranium. All the sutures were assumed to have identical isotropic linear elastic material behavior that varied in different modeling experiments, representing either fused or unfused sutures. The values of elastic moduli employed in these trials ranged over several orders of magnitude. Each model was evaluated under incisor, premolar, and molar biting conditions. Results demonstrate that skulls with unfused sutures permitted more deformations and experienced higher total strain energy. However, strain patterns remained relatively unaffected away from the suture sites, and bite reaction force was likewise barely affected. These findings suggest that suture elasticity does not substantially alter load paths through the macaque skull or its underlying rigid body kinematics. An implication is that, for the purposes of finite element analysis, omitting or fusing sutures is a reasonable modeling approximation for skulls with small suture volume fraction if the research objective is to observe general patterns of craniofacial biomechanics under static loading conditions. The manner in which suture morphology and ossification affect the mechanical integrity of skulls and their ontogeny and evolution awaits further investi-

Grant sponsor: National Science Foundation HOMINID; Grant numbers: 0725183, 0725126, 0725136, 0725078, 0725122.

*Correspondence to: Qian Wang, Division of Basic Medical Sciences, Mercer University School of Medicine, 1550 College Street, Macon, GA 31207. Fax: 478-301-5487. E-mail: wang_q2@mercer.edu

Received 16 September 2009; Accepted 8 April 2010
DOI 10.1002/ar.21203
Published online 24 July 2010 in Wiley Online Library (wileyonlinelibrary.com).

gation, and their viscoelastic properties call for dynamic simulations. Anat Rec, 293:1477–1491, 2010.

Key words: elastic properties; structural stiffness; static loading; suture fusion; bone biomechanics

INTRODUCTION

Sutures are loci of craniofacial growth but potentially are also relevant to craniofacial mechanics. Numerous *in vivo* and *in vitro* strain gage experiments have identified localized elevated strains over sutures (Behrents et al., 1978; Oudhof and van Doorenmaalen, 1983; Smith and Hylander, 1985; Herring and Mucci, 1991; Herring, 1993; Jaslow and Biewener, 1995; Rafferty and Herring, 1999; Herring and Rafferty, 2000; Herring and Teng, 2000; Rafferty et al., 2003; Sun et al., 2004; Lieberman et al., 2004; Shibazaki et al., 2007; Wang et al., 2008a) suggesting that skulls with unfused sutures do not behave mechanically as rigid bodies. Although it is clear that sutures disturb local strain flow, their global impact on skull mechanics and their mechanical properties remain poorly defined. For example, the ontogeny of suture biomechanics has been investigated in localized areas, such as the zygomatic arch in pigs (Herring et al., 2005), but no direct experiments have yet been conducted to examine the overall impact of patent sutures on the skull, primarily due to methodological limitations preventing researchers from examining global skull mechanical behavior during ontogeny. Factors complicating such efforts include variation in bite forces and bite points, limited access to bone surfaces (logistical considerations preclude the attachment of strain gages to some areas, such as the hard palate), and limited knowledge concerning the degree of fusion at individual sutures (Wang et al., 2008a). However, recent applications of finite element analysis (FEA) to vertebrate skull biomechanics provide a potential solution, because this approach allows the modeling of sutures in the context of an assessment of synchronous global strain patterns (Wroe et al., 2007; Dumont et al., 2009).

FEA is an engineering technique used to examine how structures of complex design respond to external loads (e.g., Huiskes and Chao, 1983). In FEA the structure of interest (e.g., a skull) is modeled as a mesh of simple bricks and tetrahedra (finite elements) joined at nodes, the elements are assigned material properties, certain nodes are constrained against motion, forces are applied, and displacements, stresses and strains at each node and within each element are calculated. Recent advances in computer software and imaging technology have made it possible to capture and digitally reconstruct skeletal geometry with great precision, thereby facilitating the generation of detailed finite element models (FEMs) of bony structures, including non-human vertebrate crania (Rayfield et al., 2001; Castaño et al., 2002; Rayfield, 2004, 2005a,b, 2007; Richmond et al., 2005; Strait et al., 2005, 2007, 2008, 2009; Dumont et al., 2005; Wroe 2007; Wroe et al., 2007, Wroe and coworkers 2008; McHenry et al., 2007; Kupczik et al, 2007; 2009; Farke, 2008; Pierce et al., 2008; Rayfield and Milner, 2008; Bourke et al., 2008; Moreno and coworkers, 2008; Moazen et al., 2008, 2009). However, the incorporation of realistic muscle forces, bone material properties, modeling constraints, and experimental bone strain data are equally important components of FEA that are necessary to ensure biologically meaningful results (e.g., Richmond et al., 2005; Strait et al., 2005; Ross et al., 2005; Rayfield, 2007).

Recently, the impact of sutures has been more vigorously discussed and investigated using FEA in various living and fossil species (Rayfield, 2004, 2005; Kupczik et al., 2007, 2009; Wang et al., 2007b, 2008a,b; Farke, 2008; Moazen et al., 2009; Fitton et al., 2009; Jasinoski et al., 2010) and various conclusions as to their significance on local and global skull biomechanics have been reached. Some finite element models of vertebrate crania that did not include sutures have obtained reasonable results in relation to *in vivo* bone strain studies (e.g., Strait et al., 2005), but others have not, as was the case in the less refined alligator models (Metzger et al., 2005). FEA of a theropod dinosaur skull (Rayfield, 2005b) suggested the important role sutures play in a localized functional context. Kupczik et al. (2007) demonstrated the localized impact of sutures in monkey skulls, and Moazen et al. (2009) have observed a significant impact on strain energy density (SED) patterns in small animals such as lizards. Fitton et al. (2009) performed a sensitivity analysis using the same specimens as were examined by Kupczik et al. (2007, 2009) and found that the inclusion of patent sutures in their FEMs had modest effects on strain in the immediate vicinity of the sutures but as one moved away from the sutures the effects were negligible. These results are corroborated by our initial sensitivity analyses (Wang et al., 2007b, 2008b). However, the manner in which sutural fusion affects the global biomechanics of the craniofacial skeleton has not yet been systematically studied.

This study tests the hypotheses that: (1) sutures have a significant impact on global skull mechanics, and (2) the mechanical behavior and significance of sutures depends on their material properties and positions on the cranium. A macaque FE model was analyzed using four different sets of suture material properties under three different loading cases that simulate incisor, premolar, and molar biting. Mechanical data extracted from these 12 FEAs allowed an assessment of the hypotheses.

MATERIALS AND METHODS

Model Creation

The finite element model used here was built from a male subadult *Macaca fascicularis* specimen (with third molars erupting) obtained from a biological supply company after the specimen had been sacrificed for research purposes unrelated to this study (Fig. 1). This model was created based on the protocol used previously by

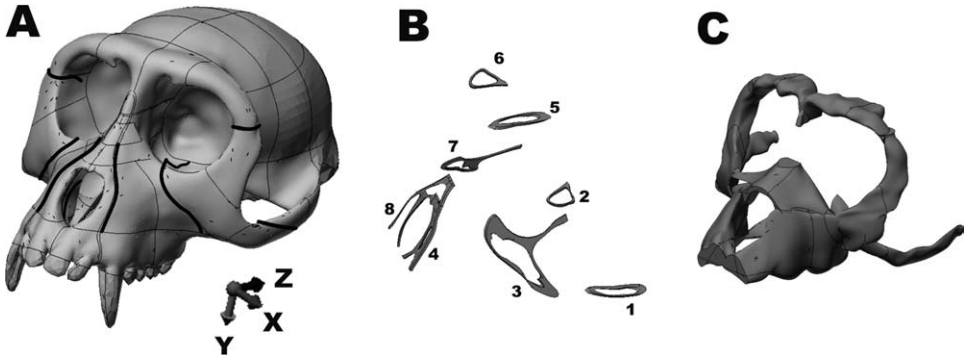

Fig. 1. Three dimensional solid model of a *M. fascicularis* skull. (**A**) Whole model with sutures highlighted. (**B**) Eight parts representing four facial sutures on left and right sides. Zygomaticotemporal suture (ZMT)– Parts 1 and 5; Zygomaticofrontal suture (ZMF)– Parts 2 and 6; Zygomaticomaxillary suture (ZMM)– Parts 3 and 7; Premaxillomaxillary suture (PMM)– Parts 4 and 8. All sutures were created to match the cortical bones that normally formed a shell over trabecular bones. The parts inside trabecular bone were omitted in order to simplify the modeling process. (**C**) Parts representing trabecular bone in the facial skeleton. They were enclosed by cortical bone.

this research group that has successfully generated realistic FEMs of monkey crania (Richmond et al., 2005; Strait et al., 2005, 2007, 2008, 2009). A tessellated surface model was constructed by first determining the optimal threshold value of the CT scans by averaging the threshold values across multiple volumes sampled throughout the facial skeleton using Quant3D (High-Resolution X-Ray CT Lab, University of Texas, Austin, http://www.ctlab.geo.utexas.edu/software/index.php), then applying the threshold to create a tessellated model of the skull using AMIRA (Visage Imaging). The tessellated surface was converted to a smooth non-uniform rational B-spline (NURBS) surface using surface editing software (Geomagic Studio 11, Geomagic, NC), which was then transformed into a solid model by using computer-assisted-design software (SolidWorks 2005, Dassault Systèmes SolidWorks). The solid was broken into 146 parts (including parts designated as sutures), each of which could potentially be assigned its own set of elastic properties (Fig. 1). The model was imported into FEA software (Algor 19, Autodesk, Pittsburg, PA) and converted into a mesh of 1,051,877 brick and tetrahedral elements that exhibited greater mesh density in the face than in the neuro- and basicranium. Suture morphology, material mechanical properties, muscle forces, constraints, and reaction forces were simulated within the three dimensional model as described later.

Parts Representing Sutures

The precise manner in which to model sutures is a serious technical challenge. Should sutures be modeled using their complex, often interdigitating morphology, or as a simplified linear corridor? Surface investigation and micro-CT image analysis have demonstrated complicated spatial variations of sutural morphology (Byron et al., 2004; Byron, 2006, 2009; Herring, 2008; Reinholt et al., 2009). Due to its pliant nature, the suture connective tissue is assumed to be able to resist mainly tensile rather than compressive loads. Therefore, bony interdigitations within sutures play a critical role in allowing external compressive loads to be absorbed as tensile forces through sutural fibers running between the inosculated sutural surfaces (Herring, 2008). Thus, sutures are better modeled as homogeneous suture-bone functional units in order to simplify this phenomenon (Farke, 2008; Wang et al., 2008b).

Four parts representing the premaxillomaxillary suture (PMM), zygomaticomaxillary suture (ZMM), zygomaticofrontal suture (ZMF), and zygomaticotemporal suture (ZMT) (Fig. 1) were created on both the left and right sides of the cranium, because these four sutures remain mostly unfused in adult monkeys (Wang et al., 2006c). As a simplifying assumption, these suture-bone units were given a uniform thickness of 1 mm, which is a coarse approximation of the breadth of the interdigitations typical in these sutures. The inferior one third of the PMM was not modeled, as it is normally closed in young adult males, even before the full eruption of the canines (Wang et al., 2006c). An explanation for such early fusion could be that forceful loading on the incisors might otherwise break off the premaxillary bone, as has been observed during *in vitro* experiments (Wang et al., 2008a). All eight sutures comprised only 0.24% of the total skull volume.

Elastic Properties of Bone and Sutures

Material properties (measures of a material's ability to resist deformation) including elastic modulus (E), and Poisson's ratio (ν), were assigned to different functional regions of the skull. Each region of the face corresponding to cortical bone was assigned its own set of isotropic elastic properties calculated from previous orthotropic elastic properties collected from rhesus macaque skulls (Wang and Dechow, 2006). Cortical regions in the neuro- and basi-cranium were assigned isotropic elastic properties based on an average of values obtained from all parts of the skull ($E = 17.3$ GPa, $\nu = 0.28$; Wang and Dechow, 2006; Wang et al., 2006b). Trabecular bone in the supraorbital torus, postorbital bar, zygomatic body and zygomatic arch was also modeled isotropically ($E = 0.64$ GPa, $\nu = 0.28$; Ashman et al., 1989). The inclusion of homogeneous parts representing trabecular bone in the finite element model appears to increase the accuracy of FEA (Castaño et al., 2002; Panagiotopoulou et al., 2010). Teeth were modeled as bone parts and were assigned the same material properties as those in

TABLE 1. Muscle forces (Newton)

	Molar	Premolar	Incisor	Orientation vector		
				x	*y*	*z*
Working-side superficial masseter	70.6	70.6	70.6	−0.2	1.0	0.2
Balancing-side superficial masseter	34.7	52.7	70.6	0.2	1.0	0.2
Working-side deep masseter	22.6	22.6	22.6	−0.6	1.0	0.0
Balancing-side deep masseter	8.2	15.4	22.6	0.6	1.0	0.0
Working-side medial pterygoid	34.8	34.8	34.8	0.75	1.0	0.0
Balancing-side medial pterygoid	6.9	20.8	34.8	−0.75	1.0	0.0
Working-side anterior temporalis	36.6	36.6	36.6	0.1	1.0	0.1
Balancing-side anterior temporalis	15.1	25.9	36.6	−0.1	1.0	0.1
Sum	229.6	279.4	329.2			

Magnitude of muscle forces for molar biting was adapted from Strait et al. (2005). While loading was confined to the incisors, the working side muscle forces of working sides were assigned to at both the working and balancing sides. In premolar loadings, muscle forces of the balancing side were in the middle of the balancing muscles forces for molar and incisor.

surrounding alveolar bone; hence periodontal ligaments were not modeled here.

The material properties to be assigned to the eight suture-bone units modeled here cannot be easily discerned. There is no consensus on the elastic modulus of sutural tissue, as indicated by widely varying published data. For example, 1.2 MPa (Kupczik et al., 2009), 10 MPa (Moazen et al., 2009), 50 MPa (Odame et al., 2005), 0.4 GPa (Farke, 2008), and 0.5-2.5 GPa (Wang et al., 2008b) have each been proposed as proper elastic moduli [1 MPa (MegaPascal) = 10^6 N/m^2; 1 GPa (GigaPascal) = 10^9 N/m^2]. Direct mechanical experiments on mammalian cadaver material of varying sizes have yielded comparably low magnitudes of elastic stiffness for sutural tissues. Elastic moduli from facial sutures in rabbits are in the range of 1.2–2.1 MPa (Radhakrishnan and Mao, 2004) while internasal sutures in ewes are 0.9 MPa (Meunier et al., 2009). However, based on strain gage experiments, these values might understate the stiffness of sutural structure. *In vivo* and *in vitro* experiments in pigs, rabbits, and monkey skulls show that average strain values in patent sutures are an order of magnitude higher than in adjacent regions of cortical bone (Herring and Mucci, 1991; Herring and Teng, 2000; Lieberman et al., 2004; Wang et al., 2008a). Thus, theoretically, the suture along with its interaction with bone fronts as a structure could exhibit elastic stiffness about one tenth that of the adjacent bones (Wang et al., 2008b). Farke (2008) proposed that the suture with the surrounding bone be considered a single functional unit which helps avoid modeling internal sutural complexity. According to this logic, the elastic moduli of sutures in monkey skulls might be expected to be around 0.5-2.5GPa, about 200 to 500 times stiffer than results obtained from mechanical tests that evaluated only the craniofacial suture connective tissue. Thus, in the present study, suture material properties were varied across a wide range of values.

Sutures were assigned isotropic material properties that varied between modeling experiments. Four different sets of mechanical properties were used for suture-bone functional units: (1) no suture or fused suture with $E = 17.3$ GPa and $\nu = 0.28$; (2) stiff suture/bone structure with $E = 1.0$ GPa; (3) less stiff suture/bone structure with $E = 50.0$ MPa, (4) least stiff suture/bone structure with $E = 1.0$ MPa. In all suture modeling experiments, Poisson's ratio was set to 0.4.

Muscles Forces and Constraint Designs

A constraint regime, or reaction loading procedure, was applied to the model. To examine the strain patterns of the skull incurred from biting on different teeth, nodes at the right and left articular eminences in the temporomandibular joint (TMJ) and at a bite point (incisors, premolars, or molars) were fixed to prevent movement of the model. When muscle forces are applied to a model with these constraints, the model is pulled inferiorly onto the fixed points, thus generating a reaction force at the bite point and the articular eminences.

In molar loading experiments, the bite point was set at all of the left (working-side) upper molar tooth crown surfaces. In premolar loading, the bite point was defined by constraining nodes on the surfaces of the left P^3 and P^4 tooth crowns. In incisor loading experiment, the bite point was defined by simultaneously constraining nodes on the surfaces of the I^1 and I^2 tooth crowns.

Eight muscle forces, generalized from previous studies (Strait et al., 2005, 2007, 2008, 2009), were applied to the model, representing the right and left anterior temporalis, superficial masseter, deep masseter and medial pterygoid (Table 1). These muscles are principally responsible for jaw elevation during mastication and they reflected their relative magnitudes when biting on different teeth. When biting at a parasagittal bite-point such as at the premolars or molars, working and balancing side muscle forces differ to eliminate distraction of the mandibular condyle at the working-side TMJ (Greaves, 1978; Spencer, 1998). When loading was confined to the incisors, the working side muscle forces magnitudes were assigned to the working and balancing side equally. In premolar loadings, muscle forces of the balancing side were in the middle of the balancing side muscle forces for molar and incisor loadings. Thus, overall applied muscle forces increased as bite points moved mesially (anteriorly). In all experiments, regardless the magnitude of total loading forces, individual loading forces were distributed on the same 1280 nodes.

Modeling Experiments

It has been suggested that different loading positions will induce different strain patterns in facial skeletons

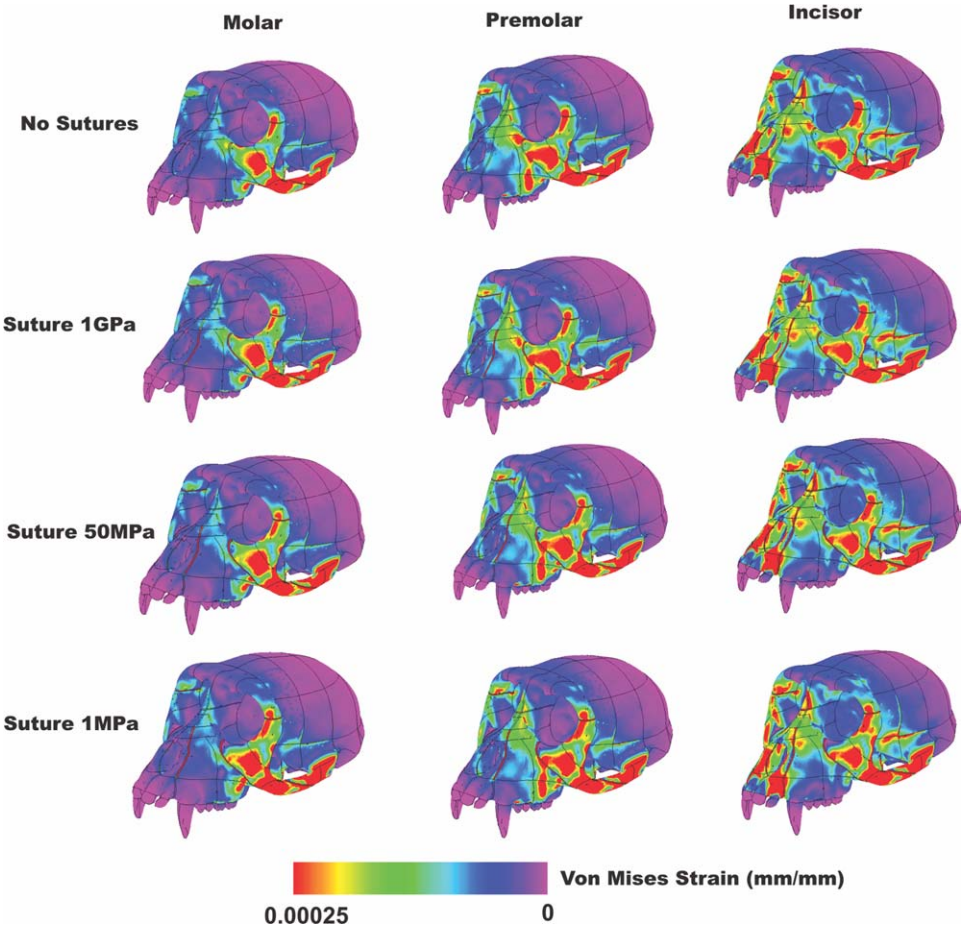

Fig. 2. Von Mises strain (unit: mm/mm) in four sutures models under three different loadings. In each loading regime, all four suture models displayed similar strain patterns, though strains over statures were higher in three models with sutures (1 GPa, 50 MPa, and 1 MPa) than in no suture or fused suture models (17.3 GPa).

(Strait et al., 2008; Kupczik et al., 2009; Wang et al., 2010b). Thus facial sutures might have different functional effects during different loading scenarios. Consequently, sutures were evaluated under varying loading conditions corresponding to bites on different sets of teeth. Experiments simulating three types of bites (incisor, premolar, molar) were performed to examine the strain patterns of bone and sutures in a monkey model with four different sets of suture elastic properties. In each type of bite, four analyses were conducted that included: no sutures, sutures with an elastic modulus of 1 GPa, 50 MPa, and 1 MPa. Thus, in total, 12 modeling experiments were performed.

For each experiment, several types of data were collected or calculated. For overall behavior of the skull, total strain energy (the total work done on the skull by the applied forces calculated as half of the sum of force multiplied by displacement: $W = {}^1/_2 * \sum^{N}_{i=1} F_i * d_i$. In this study: N = 1280). It is noteworthy that this was an approximation of the total work, since nodal force magnitudes were multiplied by nodal displacement magnitudes, instead of taking the vector product between nodal force vectors and nodal displacements. The approximate method will equal the exact work done in the case when the displacements at the nodes are exactly parallel to the forces applied to the nodes. At twenty anthropometric landmarks, nodal mean shear strain ($\varepsilon_1 + |\varepsilon_2|$) were collected, and strain mode (ratio of the maximum principal or tensile and minimum principal or compressive strains: $\varepsilon_1 / |\varepsilon_2|$) were calculated. Further, data on nodal maximum principal strain orientation (ε_1°) and reaction forces at the left and right TMJs and bite points were collected for the premolar loading experiments. Finally, ratios of strain over sutures to those over bone surfaces were calculated by dividing the maximum shear strain values on sutures by the mean of maximum shear strain values over four adjacent bone surfaces. This allows an assessment of whether the suture-bone unit is behaving realistically; previously, a suture versus bone ratio of 7.3 was observed during *in vitro* loading experiments of a monkey skull (Wang et al., 2008a).

Because FEA is a deterministic process that demonstrates the influence of different variables on the model, strain energy and other data derived from FEA violate the assumption of random sampling implicit in such tests. As a result, statistical tests were not conducted. Rather, a series of paired comparisons among the data collected from different experiments at different

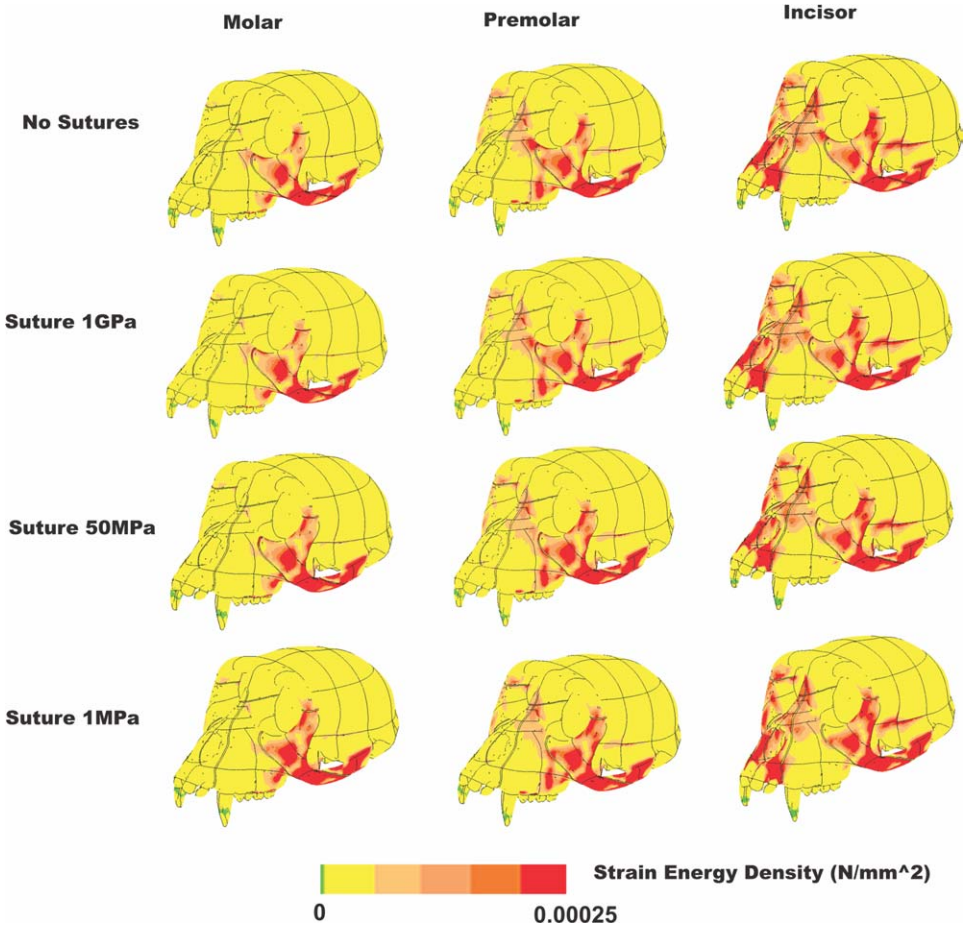

Fig. 3. Strain Energy Density (SED) (Unit: N/mm^2) in four sutures models under three different loadings. In each loading regimes, all four suture models displayed similar SED patterns. SEDs over sutures were comparable to adjacent bones in three models with sutures (1 GPa, 50 MPa, and 1 MPa) as in no suture or fused suture models (17.3 GPa).

locations on the skull were conducted to assess quantitative differences in strain magnitude, mode, and strain orientations. Results of the no-suture model were used as the reference datum for all comparisons. These comparisons were supplemented with visual comparisons of strain and SED across the entire model.

RESULTS

Overall Strain Patterns: Magnitude, Mode, and Orientations

Overall, strain patterns on bone surfaces are similar in each loading case regardless of suture material properties (Figs. 2, 3). The distribution of "hot spots" (concentrations of elevated strain or SED) remained mostly the same. For example, during all premolar loading experiments, high strain and SED were found in the area above the alveolar process extending antero-posteriorly from P^3 to M^3, and in the area above and lateral to the piriform aperture (Figs. 2, 3), comparable to those in validated FEM of monkey crania under premolar loadings (Strait et al., 2008). The only notable exception is that increasing sutural stiffness was associated with the appearance of a hot spot just below the inferomedial margin of the working-side orbit. In terms of strain magnitudes, the strains on models with sutures had, on average, slightly higher strain magnitudes than in models with fused sutures; across twenty nodes, the average maximum shear strain values increased by approximately 1%–4% as suture stiffness decreased in all loading cases (Table 2). However, at particular nodes, strain magnitude could either increase or decreases as suture stiffness changed, and in some cases these changes were considerable. Nonetheless, the average absolute change in strain magnitude was modest, ranging from approximately 4%–21%. In contrast, the changes in strain mode and strain orientation due to sutural stiffness were negligible (Table 3). Average absolute differences in strain mode did not exceed 6%, and average angular differences in the orientation of maximum principal strain were no more than 3°. Collectively, these data indicate that sutural stiffness has a minor effect on strain magnitude but not the basic nature of the strains. Finally, nodal displacements increased corresponding to the overall increase of the total strain energy, indicating a decrease in overall skull stiffness corresponding to the decrease in sutural stiffness (Tables 3, 4).

TABLE 2. Proportional change of mean nodal shear strain magnitudes ($\varepsilon_1 + |\varepsilon_2|$) compared to the no suture model

Site	Node	Molar loading (%)			Premolar loading (%)			Incisor loading (%)		
		1 GPa	50 MPa	1 MPa	1 GPa	50 MPa	1 MPa	1 GPa	50 MPa	1 MPa
Opisthokranion (op)	56,316	−7.1	−21.4	−21.4	−3.6	−10.7	−14.3	−2.0	−5.9	−5.9
Basion (ba)	19,043	0.2	−1.8	−3.1	0.2	−1.1	−1.9	−0.1	−1.2	−1.8
Staphylion (sta)	28,607	−0.6	−8.7	−13.8	0.6	−5.9	−10.9	1.6	−3.2	−7.8
Glabella (g)	40,158	−0.9	1.8	4.4	−1.1	−0.7	0.0	−1.2	−1.7	−1.2
Left midsupraorbit	5,397	1.9	13.4	21.7	1.0	8.9	16.0	3.3	11.4	16.6
Right midsupraorbit	83,904	4.9	18.9	25.9	5.0	17.1	23.2	3.4	13.0	18.1
Left infraorbital rim	33,437	−7.3	−30.9	−40.4	−6.9	−22.6	−28.0	−4.2	−17.7	−22.6
Right infraorbital rim	77,458	−7.7	−28.9	−37.8	−6.3	−24.0	−31.5	−5.8	−18.4	−23.2
Rhinion (rhi)	63,226	0.9	−12.8	−18.5	2.3	−7.4	−11.7	−2.2	−14.1	−18.5
Left center of zygoma	24,696	3.2	8.2	11.4	3.2	8.0	11.5	4.7	11.2	15.3
Right center of zygoma	13,276	7.1	14.8	16.0	8.1	18.1	20.3	8.2	19.4	22.1
Left alveolar above P3	88,338	−1.0	−0.6	−1.3	−0.4	−2.3	−4.4	2.6	1.1	0.0
Right alveolar above P3	10,195	−11.8	−31.4	−35.3	−12.6	−24.4	−26.7	−1.2	−6.6	−9.6
Prosthion (pr)	68,003	0.0	−6.6	−11.7	−0.2	−5.7	−8.8	−0.4	−0.6	−0.5
Left post zygomatic arch	139,760	18.3	59.7	76.6	15.7	50.3	64.2	12.4	36.8	45.9
Right post zygomatic arch	7,007	6.2	22.3	28.6	6.0	21.0	27.0	6.1	20.7	26.5
Left Zygomatic arch mid upper border	44,394	1.0	−2.5	−5.7	0.7	−3.7	−7.1	0.6	−3.9	−7.2
Right Zygomatic arch mid upper border	106,154	−0.2	0.7	4.1	−0.6	0.1	3.5	−1.6	−2.0	1.5
Left Zygomatic arch mid lower border	103,026	5.9	15.2	18.3	6.1	15.2	18.0	6.5	15.2	17.7
Right Zygomatic arch mid lower border	50,520	12.0	25.3	29.4	12.9	27.1	31.3	13.4	28.3	32.2
Mean		1.2	1.7	2.4	1.5	2.9	3.5	2.2	4.1	4.9
SD		6.9	22.0	27.9	6.5	18.5	23.4	5.1	14.9	18.7
Mean of absolute values		4.9	16.3	21.3	4.7	13.7	18.0	4.1	11.6	14.7
SD of absolute values		4.9	14.5	17.6	4.7	12.3	14.7	3.7	9.9	12.1

Total Strain Energy and Strain Energy Absorbed by Suturess

Total strain energy increased as sutural stiffness decreased under all loading conditions, and these differences were accentuated as the bite point moved from mesial to distal (i.e., incisor vs. premolar vs. molar; Table 4; Fig. 4).

Due to their small volume as a percentage of skull volume (0.24%), sutures only absorbed a small amount of energy. For example, in the 50 MPA model under premolar loading, only 2.47% of total strain energy (0.08 N*mm in total) was absorbed by sutures. The rest of the facial skeleton, including cortical and trabecular bone lumped together, absorbed 93.96% of the model's total strain energy (Table 5). However, sutures did absorb more energy when the sutural stiffness decreased. For example, in premolar loading analyses, all eight facial sutures absorb 0.02 N*mm in total in the no-suture model, 0.05 N*mm (2.5 times higher than in the no suture model) in the 1 GPA model, 0.08 N*mm in total (4 times higher) in the 50 MPa model, and 0.16 N*mm in total (8 times higher) in the 1 MPA model. Yet the increase of energy absorption is not proportional to the extent of the decrease in sutural stiffness. For example, in premolar loadings, facial sutures in the 1MPa suture model absorbed 3.2 times as much energy as they did in the 1 GPa suture model, even though their stiffness was three orders of magnitude less.

Reaction Forces and Biting Efficiency

The reaction force at the TMJs increased as suture stiffness decreased, while bite forces (reaction forces at the bite points) slightly decreased. For example, in premolar loadings (Table 6), at the right TMJ the reaction force increased 10.75% in the 50 MPa model, and 14.38% in the 1 MPa model relative to the no-suture model, while bite force was 1.29% lower in the 50 MPa model, and 2.05% in the 1 MPa model. Taken together, these findings indicate a slight decrease in biting efficiency as suture stiffness decreases. A premolar bite force of about 75N was generated from a total applied muscular force of 279.4N. In terms of total muscular force, the premolar biting efficiency, defined as the relationship between the tooth reaction forces and the total force exerted by the muscles, was 26.85% in the no suture model, and it was 26.30% in the 1 MPa model (Table 7). This value was smaller than theoretical values (around 38%, Dechow and Carlson, 1990), possibly because the TMJs may have been overconstrained in our model and did not allow sufficient rotation around a medio-lateral axis.

Strain Patterns Over Suture and Adjacent Bone Surfaces

Strains at the sutures were higher overall in models with sutures than in the model without sutures in all three loading scenarios, and higher in the 1 MPa and 50 MPa models than in 1 GPA models (Fig. 2; Table 8). However, the bone surfaces close to four suture sites typically exhibited only slight increases in magnitude from no suture model to 1MPa suture model (Table 8). The states of strain mode (i.e., primarily tensile strains vs. primarily compressive strains) normally did not change

TABLE 3. Change of nodal strain mode ($\varepsilon_1/|\varepsilon_2|$) (%), maximum nodal strain orientation ($\varepsilon_1\circ$), and nodal displacement under premolar loading compared to the no suture model (%)

Site	States of strain mode in no suture model[a]	Change in magnitude of strain mode (%)			Change in maximum strain orientation[b]			Change in displacement magnitude (%)		
		1 GPa	50 MPa	1 MPa	1 GPa	50 MPa	1 MPa	1 GPa	50 MPa	1 MPa
Opisthokranion (op)	C	0.0	3.0	3.0	0.0°	1.2°	1.8°	2.6	13.2	15.8
Basion (ba)	T	0.0	−0.5	−1.1	0.0°	0.0°	0.0°	0.0	0.0	0.0
Staphylion (sta)	T	0.4	0.8	1.7	0.0°	0.0°	2.8°	2.2	2.2	4.3
Glabella (g)	C	0.0	−1.4	−2.9	0.0°	0.2°	0.3°	1.5	5.9	8.8
Left midsupraorbit	T	−0.5	−4.3	−4.6	1.9°	1.9°	1.9°	2.4	9.4	12.9
Right midsupraorbit	T	−7.1	−11.5	−11.8	0.0°	0.0°	0.0°	2.4	6.1	8.5
Left infraorbital rim	T	1.0	3.6	6.8	0.0°	0.0°	0.0°	0.0	−10.0	−13.3
Right infraorbital rim	T	−0.4	−1.8	−2.5	2.7°	2.7°	2.7°	3.3	8.3	10.0
Rhinion (rhi)	T	−2.5	−4.0	−4.3	8.1°	8.1°	8.1°	4.3	10.6	12.8
Left center of zygoma	T	1.1	2.2	0.6	0.0°	5.1°	5.1°	6.2	14.4	17.5
Right center of zygoma	T	−1.7	−12.5	−17.6	0.0°	0.0°	0.0°	5.1	11.2	14.3
Left alveolar above P3	C	0.0	0.0	3.6	0.0°	0.0°	0.0°	0.0	0.0	0.0
Right alveolar above P3	C	−23.1	−26.9	−23.1	4.0°	14.8°	24.2°	3.8	8.9	10.1
Prosthion (pr)	T	−0.7	1.8	3.9	0.0°	0.4°	0.2°	6.3	15.6	18.8
Left post zygomatic arch	T	0.4	0.9	1.3	0.0°	4.5°	4.5°	7.1	28.6	35.7
Right post zygomatic arch	T	0.0	0.7	1.3	0.0°	1.1°	1.1°	11.1	22.2	22.2
Left Zygomatic arch mid upper border	C	0.0	0.0	0.0	0.0°	4.0°	4.0°	7.3	20.2	25.0
Right Zygomatic arch mid upper border	C	6.5	19.4	22.6	1.0°	2.7°	3.7°	8.4	26.2	33.8
Left Zygomatic arch mid lower border	T	0.3	1.9	2.9	0.8°	0.4°	0.0°	6.9	20.6	26.0
Right Zygomatic arch mid lower border	T	1.2	2.8	4.3	0.8°	1.7°	1.7°	9.5	26.0	31.4
Mean of absolute values[c]		2.3	5.0	6.0	1.0°	2.4°	3.1°	4.5	13.0	16.1
SD of absolute values[c]		5.3	7.1	7.1	2.0°	3.5°	5.3°	3.2	8.6	10.3

[a]The states of strain mode remained the same in the same loading regimes regardless of the stiffness of sutures (C = Compressive, T = Tensile).
[b]For the method to find the angle between two vectors, see http://www.wikihow.com/Find-the-Angle-Between-Two-Vectors.
[c]For change in strain orientation, it was angular values and angular SD respectively, calculated with the Oriana Circular Statistical Analysis Program 2.02 (Kovach Computing Services, Wales, UK) (Fig. 5).

TABLE 4. Comparison of total strain energy (total work) to the no suture model under different loading regimes. With the decrease of sutural stiffness, the overall total strain energy (an approximation of total work) in the whole skull increased, indicating a decrease of structural stiffness of the skull

Loading regime	Increase of total strain energy compared to no suture model		
	1 GPa	50 MPa	1 MPa
Molar	8%	25%	33%
Premolar	7%	20%	28%
Incisor	6%	16%	23%
Mean	7%	20%	28%
SD	1%	5%	5%

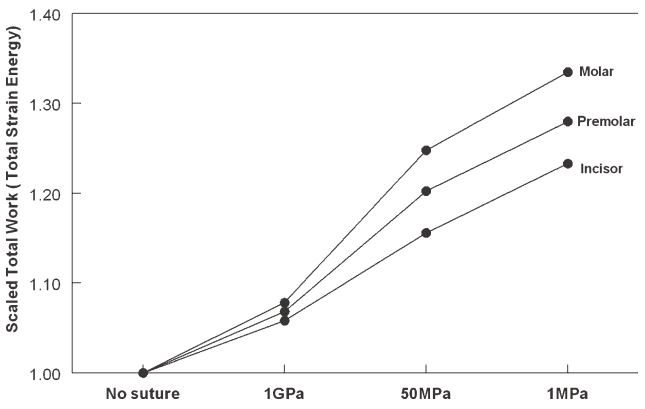

Fig. 4. Scaled total work (total strain energy) (Unit: N*mm) in four suture models under molar, premolar, and incisor loadings. The total work of the no suture model was scaled to 1. Models with sutures underwent a greater increase in total work under molar loadings, which might be related to unbalanced loading forces between the working and balancing sides.

at either sutural sites or bone surfaces, except in one of the nodes sampled anterior to the left ZMT suture. At a few sites, substantial differences in the values of strain mode could be observed (e.g., nodes near the ZMT and PMM sutures in premolar loadings) (Table 8), although these changes did not cause the basic mode of strain experienced by the node to change. The orientation of maximum principal strain ($\varepsilon_1\circ$) could change remarkably within sutures (e.g., ZMF, ZMM, and PMM), but in most cases the angular change at adjacent bone surfaces was less pronounced (Tables 3, 8).

Ratios of Strain Over Suture to Strain Over Adjacent Bone Surfaces

The ratios of sutural strain magnitude relative to magnitudes at adjacent bone surfaces varied as the stiffness of the sutures increased (Table 9). For example, in

TABLE 5. Strain energy distribution in FEA of the 50 MPa suture model under premolar loading

Analysis: 50 MPa Premolar loading	Volume (mm^3)	Percentage of total skull volume	Mean strain energy density (N/mm^2)	Total strain energy (N* mm)	Percentage of energy absorption
Face	72322.9	61.01%	4.01E-05	2.898	93.96%
Teeth	2008.2	1.69%	1.23E-06	0.002	0.08%
Cranium	43922.1	37.05%	2.45E-06	0.108	3.49%
Suture	282.8	0.24%	2.69E-04	0.076	2.47%
Sum or grand mean	118536.0	100%	2.60E-05	3.084	100%

TABLE 6. Reaction forces (Newton) and their respective vectors in principal axes at temporomandibular joints (TMJs) and left premolars in FEA of four suture models under premolar loading (Unit: Newton). Ideally, there shouldn't be any differences for a given loading condition, and differences here might be indicative of overconstraining the TMJ joint. In reality, the TMJ should be constrained so the skull can rotate freely about the TMJ if unconstrained by a bite point

	No suture	1 GPa	50 MPa	1 MPa
Left TMJ	146.70 (12.77, 82.55, 22.71)	148.69 (12.91, 82.68, 23.01)	155.27 (13.19, 82.87, 24.01)	158.15 (13.27, 82.90, 24.69)
Right TMJ	163.85 (−13.44, 80.37, 38.66)	169.08 (−14.00, 80.65, 38.17)	181.47 (−15.86, 81.64, 36.79)	187.41 (−16.90, 82.13, 36.21)
Left Premolars	75.03 (6.41, 60.88, 7.68)	74.78 (6.69, 60.49, −7.57)	74.06 (7.36, 59.77, −7.57)	73.49 (7.64, 59.31, −7.78)

all 12 analyses, the ZMF suture had the lowest overall ratio of maximum shear strains recorded at sutures against those over the adjacent bone surfaces; in the 50 MPa model, the suture/bone ratio was 1.5 at ZMF, compared to 8.0-9.5 at other suture areas.

When all sutures of the left side of the facial skeleton in 12 analyses were lumped together, the overall ratio of maximum shear strains recorded at suture against those over the adjacent bone surfaces were 3.7 in the 1GPa model, 7.3 in the 50 MPa model, and 8.1 in the 1 MPa model (Table 9). The latter two, especially in 50MPa, were close or identical to a value of 7.3 observed during *in vitro* loading experiments of a monkey skull (Wang et al., 2008a).

Variation of Strain Patterns Among and Within Sutural Parts

Sutures on the midface had different strain environments on the working and balancing sides. For example, in the 50 MPa suture model undergoing premolar loading (Table 10), the zygomaticomaxillary suture on the left or working side exhibited a compressive dominant strain regime, while on the right or balancing side, a tensile regime was found.

Within the sutures, different sections endured different strain. For example, the midpoints of four surfaces on the left ZMT suture had different strain values and modes: (1) upper and lower surfaces had higher strain than medial and lateral surfaces; (2) while the upper and medial surfaces were under compression, the lateral and lower surfaces were under tension (Fig. 6, Table 10).

DISCUSSION

Global Impact of Sutures on Skull Biomechanics

Skulls with unfused sutures have less mechanical integrity and structural rigidity than skulls with fused sutures. This is because sutures experience elevated strain and permit greater deformation of the skull. Thus, with unfused sutures, applied forces of a given magnitude produce greater strain energy compared to a skull without sutures. However, the absorption of this increase in strain energy occurs mostly in the facial skeleton. Although sutures in macaques exhibit high strains and elevated strain energy density, they do not have a high capacity, at least under static loading conditions, to absorb energy due to their limited volume. In contrast, Jaslow (1990) stated that cranial sutures in goats were able to absorb 16%–100% of energy during impact. Whether or not sutures in primates provide a significant strain-dampening or shock absorbing function under dynamic loading conditions, as suggested by Jaslow and Biewener (1995), remains to be seen. *In vivo* analyses (suture strain gage studies in *Cebus* monkeys) are currently underway and will inform our understanding of global impacts of sutures under authentic and non-static conditions (Dhabliwala et al., 2010).

Unlike strain energy, other strain patterns in the facial skeleton remained largely or moderately unchanged regardless of sutural stiffness or patency. This indicates that the presence of sutures mostly affects the structural stiffness and toughness of the facial skeleton, but does not change its general functional configuration in static loading cases. This finding likely explains why FEA of some monkey models without sutures produced general strain patterns comparable to *in vivo* experimental results (Strait et al., 2005, 2007, 2008, 2009). This suggests that primate skull models produce realistic strain results under static analysis even without incorporating sutures.

Among mammals, skulls of the Order Primates have comparatively few craniofacial sutures. Throughout evolution, many vertebrate groups have exhibited a reduction in the number of cranial bones (and associated sutures); (Rubidge and Sidor, 2001), suggesting a higher incidence of early sutural fusion. Thus, the mechanical impact of sutures may be different in animals in which either there are more sutures or sutures comprise a greater percentage of skull volume [e.g., lizards (Moazen

TABLE 7. Premolar biting force efficiency in FEA of four models under premolar loading

	No suture	1 GPa	50 MPa	1 MPa
Premolar total reaction force vs. Total muscle force assignment	26.85%	26.76%	26.51%	26.30%
Premolar total reaction force vs. Total FEA sum of force	28.93%	28.84%	28.56%	28.34%
Premolar total reaction force in Y axis vs. Total sum of force in Y axis	23.64%	23.48%	23.21%	23.03%

TABLE 8. Change of nodal shear strain magnitude (ε_{1+} $|\varepsilon_2|$), nodal strain mode ($\varepsilon_1/|\varepsilon_2|$), and nodal maximum strain orientation ($\varepsilon_1\circ$) compared to the no suture model at suture sites and over adjacent bone surfaces in premolar loading experiments

		Change in shear strain (%)			Change in strain mode (%)			Change in maximum strain orientation		
Site[a]	Node	1 GPa	50 MPa	1 MPa	1 GPa	50 MPa	1 MPa	1 GPa	50 MPa	1 MPa
Posterior 2	106,361	3	11	17	20	50	80	3.4°	5.6°	5.7°
Posterior 1	106,132	−19	−39	−41	8	8	17	1.1°	4.7°	5.1°
Left ZMT suture	64,485	339	667	704	100	192	225	1.3°	8.4°	10.6°
Anterior 1	103,374	30	36	37	−40[b]	−67[b]	−67[b]	2.4°	7.8°	5.5°
Anterior 2	102,717	−8	−3	4	11	22	39	8.6°	8.6°	5.1°
Lower 2	143,871	−3	0	7	−8	−15	−8	0°	0°	0°
Lower 1	143,986	−3	−3	3	−11	−28	−22	1.6°	3°	3°
Left ZMF suture	4,072	−26	16	36	50	25	13	23.1°	61.5°	64.4°
Upper 1	3,914	−3	−4	2	7	13	33	0°	4.5°	4.5°
Upper 2	4,951	−2	0	6	0	0	7	1.8°	1.8°	1.8°
Posterior 2	22,988	−2	−6	−2	6	6	−12	3.8°	9.6°	9.6°
Posterior 1	25,195	1	−9	−9	8	31	31	0°	3.3°	4.1°
Left ZMM suture	20,072	256	678	796	−50	−50	−33	−21.8°	−28.8°	−29°
Anterior 1	37,979	4	15	19	0	11	11	0°	0°	0°
Anterior 2	28,805	6	17	17	8	25	8	0°	0°	0°
Posterior 2	108,665	−2	−7	−9	4	12	−46	4°	6.9°	10.2°
Posterior 1	108,669	−4	−14	−17	6	0	−6	2.5°	5.4°	14°
Left PMM suture	52,608	433	1199	1444	−15	75	0	3°	11.3°	16.2°
Anterior 1	126,134	5	25	36	139	448	−22	2.8°	−2.9°	−0.1°
Anterior 2	126,278	−4	−7	−8	−25	−25	−25	12.1°	47.5°	55.3°

[a]Four bone surface nodes were selected bracketing a node on the suture, normally in the midsuture in the facial view or in the lateral view, two at each side, either upper and lower, or anterior (ant) and posterior (post) . #1 node was two elements away from the suture, and #2 was three elements further away from the suture.
[b]The states of strain mode remained the same in the same loading regimes regardless of the stiffness of sutures, except at the node anterior to the left ZMT suture (anterior 1), where it changed from tensile mode (1.5 in no suture models) to a compressive mode in suture models (0.9 in 1 GPa suture model, 0.5 in 50 MPa and 1 MPa model).

et al., 2009) and alligators (Metzger et al., 2005)]. In this light, a comparison between primates and pigs [on which many important suture experiments have been performed (i.e., Rafferty and Herring, 1999; Herring and Rafferty, 2000; Herring and Teng, 2000; Rafferty et al., 2003; Sun et al., 2004)] seems warranted. Certainly, the mechanical consequences of intertaxon variation in sutural size and morphology need careful examination.

Anterior tooth loading is associated with higher facial strain magnitudes than posterior tooth loading (Strait et al., 2008, 2009; Wang et al., 2010b), yet here the presence of sutures had a higher proportional impact during molar loadings. This might be related to increased muscle force asymmetry, which is pronounced during molar bites.

Local Impacts of Sutures and the Necessity of Modeling Sutures

Though the general strain flow and strain gradients were not changed in our analyses, strain flow could be disturbed at areas close to the sutures, as observed by other researchers (Rayfield, 2005; Fitton et al., 2009). Comparisons between different suture models revealed that the presence or absence of patent sutures has only a subtle effect on strain patterns over the whole skull, but some sizeable shifts were observed in localized areas, such as the posterior zygomatic arch and anterior midface. This suggests that the mechanical significance of sutures depends on the scale of the research questions being asked.

While the skull deflects significantly more with the flexible versus fused sutures, strain (and stress) patterns remain relatively unaffected away from the suture sites for mammalian skulls whose sutures constitute a small volume fraction. Further, suture elasticity does not substantially alter load paths through the skull, and deformations even for the most elastic sutures are still small compared to moment arms of a rigid body kinematic model of the skull. This means that the flexibility of the sutures does not affect the underlying rigid body kinematics of the structure. Otherwise, one would see

TABLE 9. Ratio of nodal mean shear strain value over the suture and over the adjacent bone surfaces on the left side of the skull

Loading regime	Suture	No suture	1 GPa	50 MPa	1 MPa
Molar	ZMT	1.0	4.2	7.8	8.0
	ZMF	1.2	0.9	1.4	1.6
	ZMM	1.5	6.2	9.9	10.8
	PMM	0.7	3.7	9.3	11.2
Premolar	ZMT	1.0	4.4	8.0	8.2
	ZMF	1.2	0.9	1.5	1.6
	ZMM	1.3	4.4	9.5	10.8
	PMM	0.6	3.5	8.6	10.2
Incisor	ZMT	1.0	4.7	8.4	8.6
	ZMF	1.2	1.0	1.7	1.8
	ZMM	1.5	5.6	10.8	11.9
	PMM	1.2	5.1	11.1	12.5
Mean		1.1	3.7	7.3	8.1
SD		0.3	1.8	3.7	4.1

Ratio of strain over sutures to those over bone surfaces were calculated by dividing mean nodal shear strain values at sutural sites by the grand mean of mean nodal shear strain values at four adjacent bone surfaces. For example, Ratio at ZMT = ZMT/[(posterior 2 + posterior 1 + anterior 1 + anterior 2)/4] (see Table 8).

different patterns of stress and strain away from the suture site due to changes in how applied forces are transmitted. Thus, it is suggested that omitting sutures in FEA is a reasonable modeling approximation for skulls with small suture volume fraction if the objective of the analysis are to obtain patterns of stress and strain of the craniofacial skeleton in general, in particular regions away from suture sites, or predict bite force. However, if a research objective is to understand fine scale strain patterns in a small bony region very close to a suture, it is clearly important to incorporate sutures into the analysis. If the objective is to understand global strain patterns across large swaths of the skull, then a consideration of sutures becomes less important.

When sutures are to be included, a suture-bone functional unit could be applied to simplifying the modeling procedure. Though the exact material properties of this artificial structure is not known yet, in contrast to certain expectations (see previous), in FEA, those with elastic moduli of 50 MPa and 1 MPa produced the suture versus adjacent bone surface strain ratios most comparable to the ratio measured in *in vitro* experiments on monkey skulls (Wang et al., 2008a). However, the 1 MPa value reflects the stiffness of sutural tissue, yet the suture-bone units modeled here are 1 mm thick, which exceeds the length of sutural fibers in primate sutures. Thus, we infer that the most reasonable modeling approach in primates (and, perhaps, comparable vertebrates) is to employ an isotropic elastic modulus for suture-bone units that is approximately 50 MPa.

Complexity in Modeling Sutures

It is worth noting that there are significant variations among and within sutures in terms of morphological complexity and internal structural configurations (Byron et al., 2004; Byron, 2006, 2009; Herring, 2008; Reinholt et al., 2009; Jasinoski et al., 2010). This variation may be due to variation in growth potentials (Massler and Schour, 1951; Ozaki et al., 1998; Opperman, 2000; Sun et al., 2004; Carmody et al., 2008; Wang et al., 2007a), dietary adaptations (Byron, 2009), genetic patterning (Wang et al., 2006a), aging processes (Gross, 1961; Milch, 1966; Miroue and Rosenberg, 1975; Kokich, 1976), fusion patterns (Wang et al., 2006c), and ontogenetic changes in material properties along with cortical bones (Wang et al., 2010a). How these variables might affect the biomechanical behavior of sutures warrants further investigation.

TABLE 10. Variations in state of strain modes within sutures in the 50 MPa suture model under premolar loading

Suture	Section	State of strain mode (ε_1 / ε_2) Left	Right
ZMT	Upper midsuture	C	C
	Lateral midsuture	T	C
	Medial midsuture	C	T
	Lower midsuture	T	T
ZMF	Facial view median part	T	T
	Facial view middle part	T	T
	Facial view lateral part	T	T
ZMM	Facial view upper part	C	T
	Facial view middle part	C	T
	Facial view lower part	C	T
PMM	Facial view upper part	C	C
	Facial view middle part	T	T
	Facial view lower part	T	C

C, compressive; T, tensile.

Role of Sutures: Growth Versus Biomechanical Integrity

The development of calvarial bones is tightly coordinated with the growth of the brain and requires interactions between different tissues within the calvarial sutures (Kim et al., 1998; Kreiborg, 2000), and is modified under the influence of masticatory hypofunction (Ulgen et al., 1997; Katsaros et al., 2002) as well hyperfunction (Byron et al., 2004). Every suture-bone interface might have its own mechanical and developmental context (Shibazaki et al., 2007; Holton et al., 2010) and fusion patterns (Wang et al., 2006c). How this diversity in sutural morphology and structure might affect and be

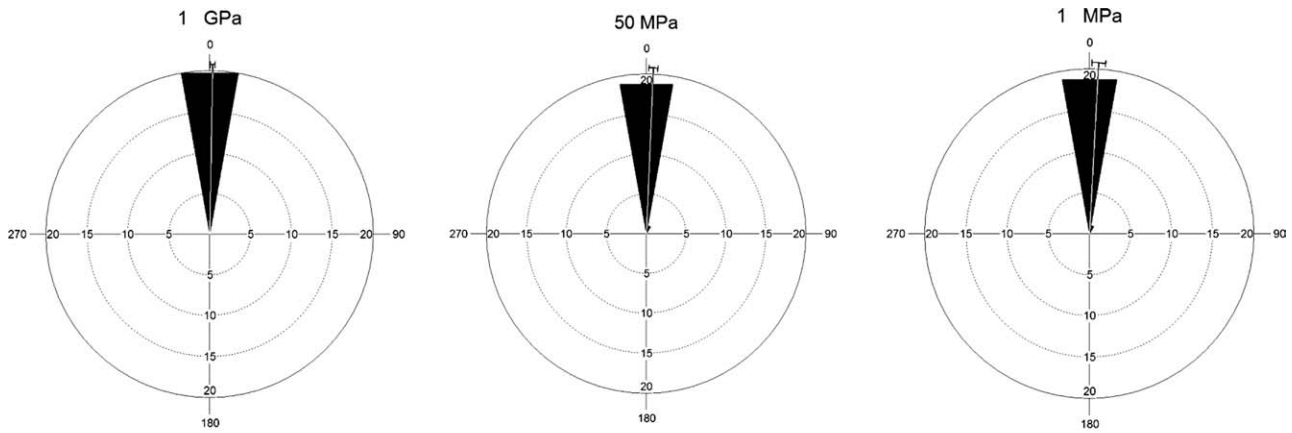

Fig. 5. Change of the orientation of principal maximum strain (ε_1^s) compared to the no suture model at 20 nodes in craniofacial skeletons. The change was very small in all suture models, though the difference was slightly bigger between no suture model and 1 MPa suture model than between no suture model and other suture models.

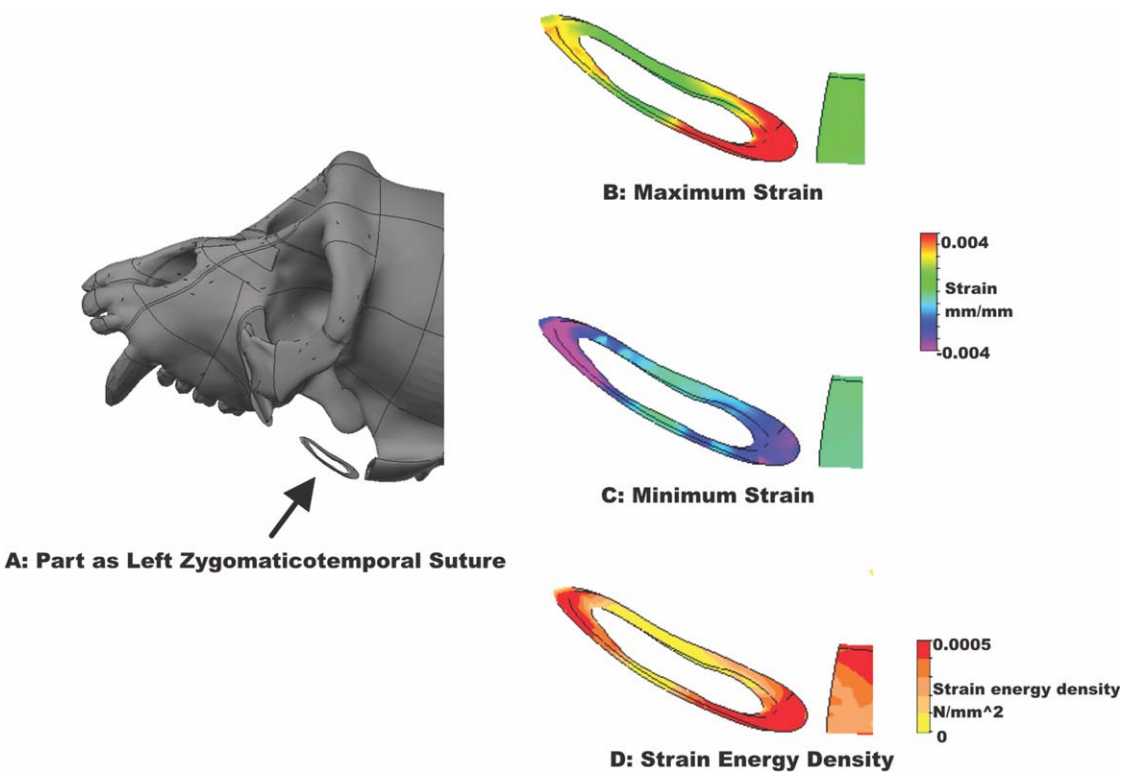

Fig. 6. Variation within the left zygomaticotemporal suture (ZMT) in the 50 MPa suture model under premolar loading. (**A**) A simplified part designed as left ZMT suture. Parts of cortical (anterior and posterior to it) and trabecular (inside its loop) bone were hidden. (**B–D**) Variations of strain and strain energy density throughout the ZMT suture. The midpoints of four surfaces at the left ZMT suture had different strain values and modes. The upper and lower sections had higher strains than medial and lateral sections. The upper and medial sections were under compression, while the lateral and lower sections were under tension. Part of the posterior zygomatic arch was present to demonstrate that sutures had relatively high strain, yet their strain energy density magnitudes were comparable to that in cortical bones.

affected by skull biomechanics also needs further study. Moreover, the manner in which they respond to the ever-changing tensile or compressive loading environments as observed in this study also awaits more investigation. Overall, one might hypothesize that a delicate balance is maintained to determine the patency and fusion of sutures during the growth of the skull, which calls for ontogenetic studies at a global level. Similarly, sutural fusion may have affected and been affected by feeding mechanics during the evolution of sutural fusion patterns in vertebrates. For example, in reptiles, over time, mammal –like reptiles exhibited a reduction in the number of cranial bones (suggesting a higher incidence of early sutural fusion), which could be associated with the evolution of mastication (Sidor, 2001; Sidor et al., 2004). Thus, the effect of patent sutures on evolution of craniofacial skeletons awaits further studies on skull biomechanics in a phylogenetic context (Wang et al., 2006c).

CONCLUSION

1. Skulls with unfused sutures had less mechanical integrity and experienced greater deformation. Sutures had the highest impact in simulations of molar loadings. As suture stiffness decreased, the total strain energy absorbed by the skull increased. Reaction forces at the temporomandibular joints (TMJ) increased in models with sutures, but the bite force decreased slightly when sutures were more compliant.
2. For simplifying suture-bone integration patterns, sutures can be modeled as suture-bone functional units. Sutures with an elastic modulus of 1–50 MPa produced the suture versus adjacent bone surface strain ratios most comparable to those measured in *in vitro* experiments on monkey skulls. There was remarkable variation among and within sutures. Sutures at opposite sides and different sections of a suture could have different strain patterns, as when one section of a suture experienced primarily tension while another section simultaneously experienced primarily compression. This is consistent with the complexity of real suture morphology, and the question of how to better model the suture-bone interface needs further investigation.
3. Overall strain patterns were similar regardless of sutural stiffness, suggesting that the flexibility of the sutures did not affect the underlying rigid body kinematics of the craniofacial skeleton. Deformations for even the most elastic sutures were still small compared to moment arms of a rigid body kinematic model of the skull. Further, elasticity of the suture did not substantially alter load paths through the skull. The shift of strain patterns on bone surfaces adjacent to sutures was generally small, except in the zygomactic arch and anterior face. The presence of zygomaticofrontal sutures had little impact on the face. Due to their small volume, the energy absorbing capacity of sutures was limited. Although high strains were observed in sutures, most of the strain energy was absorbed by the facial skeleton. These findings suggest that omitting sutures or fusing sutures in static analysis is a reasonable modeling approximation for skulls with small suture volume fraction if the objective of the analysis is to either observe global stress and strain patterns, obtain patterns of stress and strain in regions far from suture sites, or to investigate bite efficiency.

ACKNOWLEDGMENTS

The authors thank Dr. Michael Horst, Dr. Daniel Hagan, Dr. Sandra Leeper-Woodford, Dr. Pad Rengasamy, Mrs. Denise Collins, Mrs. Ernestine Waters, and Mrs. Li Sun for their various help. They also thank the editors and reviewers for providing valuable advice for improving the manuscript.

LITERATURE CITED

Ashman RB, Rho JY, Turner CH. 1989. Anatomical variation of orthotropic elastic moduli of the proximal human tibia. J Biomech 22:895–900.

Behrents RG, Carlson DS, Abdelnour T. 1978. In vivo analysis of bone strain about the sagittal suture in *Macaca mulatta* during masticatory movements. J Dent Res 57:904–908.

Bourke J, Wroe S, Moreno K, McHenry C, Clausen P. 2008. Effects of gape and tooth position on bite force and skull stress in the dingo (Canis lupus dingo) using a 3-dimensional finite element approach. PLoS ONE 3:1–5.

Byron CD, Borke J, Yu J, Pashley D, Wingard CJ, Hamrick M. 2004. Effects of increased muscle mass on mouse sagittal suture morphology and mechanics. Anat Rec A 279:676–684.

Byron CD. 2006. The role of the osteoclast in cranial suture waveform patterning. Anat Rec A 288:552–563.

Byron CD. 2009. Cranial suture morphology and its relationship to diet in *Cebus*. J Hum Evol 57:649–655.

Carmody KA, Mooney MP, Cooper GM, Bonar CJ, Siegel MI, Dumont ER, Smith TD. 2008. Relationship of premaxillary bone and its sutures to deciduous dentition in nonhuman primates. Cleft Palate-Cran J 45:93–100.

Castaño MC, Zapata U, Pedroza A, Jaramillo JD, Roldán S. 2002. Creation of a three-dimensional model of the mandible and the TMJ in vivo by means of the finite element method. Int J Comput Dent 5:87–99.

Dehabliwala J, Byron C, Ross C, Reed D, Wang Q. 2010. Sagittal suture mechanics in apelloid vs. non apelloid *Cebus* during hard-object feeding. Am J Phys Anthropol Suppl 50:94.

Dechow PC, Carlson DS. 1990. Occlusal force and craniofacial biomechanics during growth in rhesus monkeys. Am J Phys Anthropol 83:219–237.

Dumont ER, Grosse IR, Slater GJ. 2009. Requirements for comparing the performance of finite element models of biological structures. J Theoret Biol 256:96–103.

Dumont ER, Piccirillo J, Grosse IR. 2005. Finite-element analysis of biting behavior and bone stress in the facial skeletons of bats. Anat Rec A 283:319–330.

Farke AA. 2008. Frontal sinuses and head-butting in goats: a finite element analysis. 2008. J Exp Biol 211:3085–3094.

Fitton LC, Kupczik K, Milne N, Fagan MJ, O'Higgins P. 2009. The role of sutures in modulating strain distribution within the skull of *Macaca fascicularis*. Am J Phys Anthropol Suppl 48:189.

Greaves WS. 1978. The jaw lever system in ungulates: a new model. J Zool Lond 184:271–285.

Gross J. 1961. Aging of connective tissue, the extracellular components. In: Bourne GH, editor. Structural aspects of aging. New York: Hafner Publishing. p 179–192.

Herring SW. 1993. Epigenetic and functional influence on skull growth. In: Hanken J, Hall BK, editors. The vertebrate skull. Vol 1. Chicago: University of Chicago Press, p 153–206.

Herring SW. 2008. Mechanical influences on suture development and patency. In: Rice DP, editor, Craniofacial sutures. Development, disease and treatment. Vol. 12. Front Oral Biol. Basel, Karger. p 41–56.

Herring SW, Mucci RJ. 1991. In vivo strain in cranial sutures: the zygomatic arch. J Morphol 207:225–239.
Herring SW, Pedersen SC, Huang X. 2005. Ontogeny of bone strain: the zygomatic arch in pigs. J Exp Biol 208:4509–4521.
Herring SW, Rafferty KL. 2000. Cranial and facial sutures: functional loading in relation to growth and morphology. In: Davidovitch Z, Mah J, editors. Biological mechanisms of tooth eruption, resorption and replacement by implants. Boston: Harvard Society for Advanced Orthodontics. p 269–276.
Herring SW, Teng S. 2000. Strain in the braincase and its sutures during function. Am J Phys Anthropol 112:575–593.
Holton NE, Franciscus RG, Nieves MA, Marshall SD, Reimer SB, Southard TE, Keller JC, Maddux SD. 2010. Sutural growth restriction and modern human facial evolution: an experimental study in a pig model. J Anat 216:48–61.
Huiskes R, Chao EYS. 1983. A survey of finite element analysis in orthopedic biomechanics: the first decade. J Biomech 16:385–409.
Jasinoski SC, Rayfield EJ, Chinsamy A. 2010. Functional implications of dicynodont cranial suture morphology. J Morphol 271:705–728.
Jaslow CR. 1990. Mechanical properties of cranial sutures. J Biomech 23:313–321.
Jaslow CR, Biewener AA. 1995. Strain patterns in the horncores, cranial bones and sutures of goats (*Capra hircus*) during impact loading. J Zool 235:193–210.
Katsaros C, Berg R, Kiliaridis S. 2002. Influence of masticatory muscle function on transverse skull dimensions in the growing rat. J Orofac Orthop 63:5–13.
Kreiborg S. 2000. Postnatal growth and development of the craniofacial complex in premature craniosynostosis. In: Cohen MM, Jr, editor. Craniosynostosis, diagnosis, evaluation and management. New York: Oxford University Press. p. 81–103.
Kim HJ, Rice DPC, Kettunen PJ, Thesleff I. 1998. FGF-, BMP- and Shh-mediated signalling pathways in the regulation of cranial suture morphogenesis and calvarial bone development. Development 125:1241–1251.
Kokich VG. 1976. Age changes in the human frontozygomatic suture from 20 to 95 years. Am J Orthod 69:411–430.
Kupczik K, Dobson CA, Fagan MJ, Crompton RH, Oxnard CE, P. O'Higgins. 2007. Assessing mechanical function of the zygomatic region in macaques: validation and sensitivity testing of finite element models. J Anat 210:41–53.
Kupczik K, Dobson CA, Crompton RH, Phillips R, Oxnard CE, Fagan MJ, O'Higgins P. 2009. Masticatory loading and bone adaptation in the supraorbital torus of developing macaques. Am J Phys Anthropol 139:193–203.
Lieberman DE, Krovitz GE, Yates FW, Devlin M, Claire MS. 2004. Effects of food processing on masticatory strain and craniofacial growth in a retrognathic face. J Hum Evol 46:655–677.
Massler M, Schour I, 1951. The growth pattern of the cranial vault in the albino rat as measured by vital staining with alizarine red S. Anat Rec 110:83–101.
McHenry CR, Wroe S, Clausen PD, Moreno K, Cunningham E. 2007. Supermodeled sabercat, predatory behavior in Smilodon fatalis revealed by high-resolution 3D computer simulation. Proc Natl Acad Sci USA 104:16010–16015.
Metzger KA, Daniel WJT, Ross CF. 2005. Comparison of beam theory and finite-element analysis with in vivo bone strain data from the alligator cranium. Anat Rec A 283:331–348.
Meunier E, Gilbert C, Byron CD, Wang Q. 2009. Effect of temperature on tensile structural elasticity of facial sutures in ewes (*Arius gigas*): a preliminary comparison between room temperature and body temperature. In: Proceedings of the Mercer University Undergraduate Research Symposium, Macon, GA; April 17, 2009; Book of Abstracts; pp 31–32.
Milch RA. 1966. Aging of connective tissues. In: Schock NW, editor. Perspectives in experimental gerontology. Springfield: Charles C Thomas. p 109–124.
Miroue M, Rosenberg L. 1975. The human facial sutures: a morphological and histological study of age changes from 20 to 95 years. M.S.D. thesis. University of Washington, Washington.
Moazen M, Curtis N, Evans SE, O'Higgins P, Fagan MJ. 2008. Combined finite element and multibody dynamics analysis of biting in a Uromastyx hardwickii lizard skull. J Anat 2135:499–508.
Moazen M, Curtis N, O'Higgins P, Jones ME, Evans SE, Fagan MJ. 2009. Assessment of the role of sutures in a lizard skull: a computer modelling study. Proc Biol Sci 276:39–46.
Odame P, Yu JC, Zhang G. 2005. 3D Finite Element study of stress distribution at the cranial bone/suture interface. Trans Soc Biomater 26:556.
Opperman LA. 2000. Cranial sutures as intramembranous bone growth sites. Dev Dyn 219:472–485.
Ozaki W, Buchman SR, Muraszko KM, Coleman D. 1998. Investigation of the influences of biomechanical force on the ultrastructure of human sagittal craniosynostosis. Plast Reconstructive Surg 102:1385–1394.
Oudhof HA, Van Doorenmaalen WJ. 1983. Skull morphogenesis and growth: hemodynamic influence. Acta Anat (Basel) 117:181–186.
Panagiotopoulou O, Curtis N, Higgins PO, Cobb SN. 2010. Modelling subcortical bone in finite element analyses: a validation and sensitivity study in the macaque mandible. J Biomech 43:1603–1611.
Pierce SE, Angielczyk KD, Rayfield EJ. 2008. Patterns of morphospace occupation and mechanical performance in extant crocodilian skulls: a combined geometric morphometric and finite element modeling approach. J Morphol 269:840–864.
Radhakrishnan P, Mao JJ. 2004. Nanomechanical properties of facial sutures and sutural mineralization front. J Dent Res 83:470–475.
Rafferty KL, Herring SW. 1999. Craniofacial sutures: morphology, growth, and in vivo masticatory strains. J Morphol 242:167–179.
Rafferty KL, Herring SW, Marshall C. 2003. The biomechanics of the rostrum and the role of facial sutures. J Morph 257:33–44.
Rayfield EJ, Norman DB, Horner CC, Horner JR, Smith PM, Thomason JJ, Upchurch P. 2001. Cranial design and function in a large theropod dinosaur. Nature 409:1033–1037.
Rayfield EJ. 2004. Cranial mechanics and feeding in *Tyrannosaurus rex*. Proc R Soc Lond (Biol) 271:1451–1459.
Rayfield EJ. 2005a. Aspects of comparative cranial mechanics in the theropod dinosaurs *Coelophysis, Allosaurus and Tyrannosaurus*. Zool J Linn Soc 144:309–316.
Rayfield EJ. 2005b. Using finite-element analysis to investigate suture morphology: a case study using large carnivorous dinosaurs. Anat Rec 283:349–365.
Rayfield EJ. 2007. Finite element analysis and understanding the biomechanics and evolution of living and fossil organisms. Annu Rev Earth Planet Sci 35:541–576.
Rayfield EJ, Milner AC. 2008. Establishing a framework for archosaur cranial mechanics. Paleobiology 34:494–515.
Reinholt LE, Burrows AM, Eiting TP, Dumont ER, Smith TD. 2009. Histology and Micro CT as methods for assessment of facial suture patency. Am J Phys Anthropol 138:499–506.
Richmond BG, Wright BW, Grosse I, Dechow PC, Ross CF, Spencer MA, Strait DS. 2005. Finite element analysis in functional morphology. Anat Rec A 283:259–274.
Ross CF, Patel BA, Slice DE, Strait DS, Dechow PC, Richmond BG, Spencer MA. 2005. Modeling masticatory muscle force in finite element analysis: sensitivity analysis using principal coordinates analysis. Anat Rec A 283:288–299.
Rubidge BS, Sidor CA. 2001. Evolutionary patterns among Permo-Triassic therapsids. Annu Rev Ecol Syst 32:449–480.
Shibazaki R, Dechow PC, Maki K, Opperman LA. 2007. Biomechanical strain and morphologic changes with age in rat calvarial bone and sutures. Plast Reconstr Surg 119:2167–2178.
Sidor CA. 2001. Simplication as a trend in synapsid cranial evolution. Evolution 58:1419–1442.
Sidor CA, Hopson JA, Keyser AW. 2004. A new burnetiamorph therapsid from the Teekloof formation Permian of South Africa. J Vert Paleontol 24:938–950.
Smith KK, Hylander WL. 1985. Strain gauge measurement of mesokinetic movement in the lizard *Varanus exanthematicus*. J Exp Biol 114:53–70.

Spencer MA. 1998. Force production in the primate masticatory system: electromyographic tests of biomechanical hypotheses. J Hum Evol 34:25–54.

Strait DS, Richmond BG, Spencer MA, Ross CF, Dechow PC, Wood BA. 2007. Masticatory biomechanics and its relevance to early hominid phylogeny: an examination of palatal thickness using finite-element analysis. J Hum Evol 52:585–599.

Strait DS, Wang Q, Dechow PC, Ross CF, Richmond BG, Spencer MA, Patel BA. 2005. Modeling elastic properties in finite element analysis: how much precision is needed to produce an accurate model? Anat Rec A 283:275–287.

Strait DS, Weber GW, Neubauer S, Chalk J, Richmond BG, Lucas PW, Spencer MA, Schrein C, Dechow PC, Ross CF, Grosse IR, Wright BW, Constantino P, Wood BA, Lawn B, Hylander WL, Wang Q, Byron CD, Slice DE, Smith AL. 2009. The feeding biomechanics and dietary ecology of *Australopithecus africanus*. Proc Natl Acad Sci USA 106:2124–2129.

Strait DS, Wright BW, Richmond BG, Ross CF, Dechow PC, Spencer MA, Wang Q. 2008. Craniofacial strain patterns during premolar loading: implications for human evolution. In: Vinyard CJ, Ravosa MJ, Wall CE, editors. Primate craniofacial function and biology, Development in primatology series. New York: Springer. p 173–198.

Sun Z, Lee E, Herring SW. 2004. Cranial sutures and bones: growth and fusion in relation to masticatory strain. Anat Rec A 276:150–161.

Ulgen M, Baran S, Kaya H, Karadede I. 1997. The influence of masticatory hypofunction on craniofacial growth and development in rats. Am J Orthod Dentofac Orthop 111:189–198.

Wang Q, Ashley DW, Dechow PC. 2010a. Regional, ontogenetic, and sex-related variations in elastic properties of cortical bone in baboon mandibles. Am J Phys Anthropol 141:526–549.

Wang Q, Dechow PC. 2006. Elastic properties of external cortical bone in the craniofacial skeleton of the rhesus macaque. Am J Phys Anthropol 131:402–415.

Wang Q, Dechow PC, Hens SM. 2007a. Ontogeny and diachronic changes in sexual dimorphism in the craniofacial skeleton of rhesus macaques from Cayo Santiago, Puerto Rico. J Hum Evol 53:350–361.

Wang Q, Dechow PC, Wright BW, Ross CF, Strait DS, Richmond BG, Spencer MA, Byron CD. 2008a. Surface strain on bone and sutures in a monkey facial skeleton: an in vitro method and its relevance to finite element analysis. In: Vinyard CJ, Ravosa MJ and Wall CE, editors. Primate craniofacial function and biology. Developments in primatology series. New York: Springer. p 149–172.

Wang Q, Opperman LA, Havill LM, Carlson DS, Dechow PC. 2006a. Inheritance of sutural pattern at the pterion in rhesus monkeys skulls. Anat Rec A 288:1042–1049.

Wang Q, Strait DS, Dechow PC, 2006b. A comparison of cortical elastic properties in the craniofacial skeletons of three primate species and its relevance to the study of human evolution. J Hum Evol 51:375–382.

Wang Q, Strait DS, Dechow PC. 2006c. Fusion patterns of craniofacial sutures in rhesus monkey skulls of known age and sex from Cayo Santiago. Am J Phys Anthropol 131:469–485.

Wang Q, Strait DS, Smith AL, Chalk J, Wright BW, Dechow PC, Richmond BG, Ross CF, Spencer MA. 2007b. Crossing the lines: suture biomechanics in the primate craniofacial skeleton examined using finite element analysis. Am J Phys Anthropol Suppl 44:243.

Wang Q, Strait DS, Smith AL, Chalk J, Wright BW, Dechow PC, Richmond BG, Ross CF, Spencer MA, Byron CD, Lucas P, Grosse I, Slice DE, Weber G. 2008b. Modeling the elastic properties of sutures in finite element analysis. Am J Phys Anthropol Suppl 46:217–218.

Wang Q, Wright BW, Smith A, Chalk J, Byron CD. 2010b. Mechanical impact of incisor loading on the primate midfacial skeleton and its relevance to human evolution. Anat Rec 293:607–617.

Wroe S, Moreno K, Clausen P, McHenry C, Curnoe D. 2007. High-resolution three-dimensional computer simulation of hominid cranial mechanics. Anat Rec 290:1248–1255.